Title

Endoplasmic reticulum transport of glutathione by Sec61 is regulated by Ero1 and Bip

By

Alise Ponsero, Aeid Igbaria, Maxwell A. Darch, Samia Miled, Caryn E. Outten, Jakob R. Winther, Benoit D'autreaux, Agnes Delaunay-Moisan and Michel B. Toledano

Supplemental information

Supplemental methods

1. Strains, plasmids and growth conditions

Strains and plasmids are listed in supplementary Table S1 and S2. The strains used in this study are derivative of BY4741, BY4742 or, as indicated in Table S1. Cells were cultured at 30 °C, or as indicated, in YPD (1% yeast extract, 2% peptone and 2% glucose), or minimal media (SD) (0.67% yeast nitrogen base w/o amino acids, 2% glucose) amino-acid supplements, as appropriate. Glutathione, diamide, dithiothreithol, puromycin, cycloheximide, and methoxypolyethylene glycol maleimide (PEG-maleimide) 2,000 and 5,000 were purchased form SIGMA. pRS304-ER-rxYFP-Grx1 was constructed by PCR-based fusion of the Mns1 ER targeting sequence at the 5'-end and of the HDEL retention signal sequence at the 3'-end of cytosolic rxYFP-Grx1 (Bjornberg et al., 2006). The Mns1-rxYFP-Grx1-HDEL DNA fusion was then integrated between the *Mlu*I and *Spe*I sites of pRS304, downstream to the *PGK1* promoter, thus replacing the entire ER-rxYFP sequence in pHOJ150 (Ostergaard et al., 2004). pRS315-ER-rxYFP was constructed by subcloning the coding sequence of ER-rxYFP from pHOJ150 (Ostergaard et al., 2004) between the *Not*I and *Sac*II sites of pRS315. pRS315-Cyt-rxYFP was similarly constructed by subcloning the Cyt-rxYFP coding sequence from pJH208 (Hu et al., 2008) into pRS315 The ER-1-Cys-Grx1 probe was synthesized (Eurofins MWG Operon) by fusion from the 5'-end the *MNS1* signal sequence, three copies of the Myc tag sequence, the yeast *GRX1* sequence carrying a Cys30 to Ser substitution, and the HDEL ER retrieving signal sequence. The fusion gene was cloned between the *Bam*HI and *Hind*III sites of pTEF415, downstream of the TEF promoter. The Cyt-1-Cys-Grx1 probe was similarly constructed without the *MNS1* and *HDEL* sequences.

2. Glutathione enzymatic measurement

Total and oxidized glutathione were measured using the Ellman's reagent, 5,5'-dithiobis (2 nitrobenzoic acid) (DTNB, SIGMA)) colorimetric assay. Ten units (OD_{600}) of a cell suspension was washed in water, pelleted and frozen at -80°C in 1% sulfosalicylic acid (SSA). Upon thawing, cells were

disrupted by the glass beads shaking method, and kept on ice for 30 min, followed by centrifugation at 16000 rpm for 15min at 4°C, and the supernatant was recovered. For total glutathione determination, 5 to 20µl of the cell supernatant was added to the reaction buffer (0.1 M sodium phosphate, pH 7.5, 1 mM EDTA, 0.2 mM NADPH, and 0.2 mM DTNB) pre-warmed at 30°C; the reaction was initiated by addition of 1 Unit glutathione reductase (SIGMA), and the change of absorbance at 412 nm was measured using a spectrophotometer during 1 min. For GSSG determination, 2µl of 2-vinylpyridine and 2µl of 25% triethanolamine were added to 100µl of the cell supernatant, in order to raise the pH and alkylate GSH. Samples were kept 1h at room temperature, then 5-20µl were used in the DTNB recycling assay.

The cellular concentrations of total glutathione ($[GSx]_{TotCell}$) and GSSG ($[GSSG]_{TotCell}$) were determined based on a GSx and GSSG standard titration curves, and on the basis of an estimated average cell volume of 48 μm^3 and the cell number of the particular sample determined by the number of colony-forming units upon plating serial dilutions of the cell suspension on YPD-agar plates. Accordingly, measurements took into account cellular loss during experiments.

3. Glutathione tolerance and survival assays

For plate assays, tolerance to HGT1-dependent GSH toxicity was assessed by spotting 5µL on plates containing various amount of GSH via serial dilution of cell cultures in exponential growth phase.

For the GSH survival assays, cultures of exponential-phase cells were divided in two, one receiving GSH at various concentrations and the other not. At the indicated times, cells were collected, counted using a coulter counter, and spread on YPD plates at a density of approximatively 200 CFU/plate. Three independent biological replicates and at least two technical replicates were performed. Plates were incubated 3 days at 30°C and CFU were counted. The percentage of survival was calculated using the untreated culture as 100%.

4. Redox westerns

Protein extraction and alkylation were performed as previously described (Delaunay et al., 2000). For rxYFP, after cell disruption by the glass beads shaking method in the presence of trichloroacetic acid (TCA) (20% final), precipitated proteins were dissolved in SB buffer (100 mM Tris–Cl pH 8, 1% SDS) containing 50 mM N-ethylmaleimide (NEM) and incubated 1h at RT in the dark. Protein concentration was measured by bicinchoninic acid-based colorimetric detection (micro BCA kit, Pierce), and the protein sample was separated by non-reducing SDS-polyacrylamide gel electrophoresis. For 1-Cys-Grx1 and Kar2, following protein-TCA precipitation, free reduced Cys residues were alkylated with 50 mM NEM for 1h at RT in the dark, then proteins were again precipitated with TCA, and the precipitated pellet washed 3 times with cold acetone. Samples were then dissolved in sample SB buffer, incubated 15 min with 200 mM DTT and again TCA-precipitated. After three washes the protein pellet was resuspended in SB buffer containing 30 mM PEG-maleimide 5,000 (Kar2) or 2,000

(1-Cys-Grx1) for 20 min at RT in the dark. Samples were then separated by reduced SDS-PAGE. After gel electrophoresis and gel transfer, 1-Cys-Grx1 was revealed with the 9E10 anti-Myc monoclonal antibody (a gift from C. Créminon, Saclay, France), rxYFP with rabbit polyclonal anti-GFP (Life Technologies), and a Kar2-specific antibody (Santa Cruz). Primary antibodies were then revealed with anti-mouse IgG or anti-rabbit IgG secondary antibodies labelled with fluorophores of different wavelengths, followed by Infrared Imaging technology (Odyssey, LI-COR). The reduced-to-oxidized ratio of rxYFP and 1-Cys-Grx1 was quantified using the LiCOR Image Studio software.

5. Calculation of redox potentials and GSH/GSSG

The reduced-to-oxidized rxYFP ratio was used to calculate E_{GSH} using the Nernst equation:

$E_{GSH} = E°'_{GSH} - (60.1\ mV/2)\ \log[GSH]^2/[GSSG] = E°'_{rxYFP} - (60.1\ mV/2)\ \log(rxYFP_{red})/(rxYFP_{ox}) = E_{rxYFP}$ (Equation 1)

With $E°'_{GSH}$ = -240 mV and $E°'_{rxYFP}$ = -265 mV, at pH 7.

The reduced-to-oxidized 1-Cys-Grx1 ratio was used to calculate R_{GS} = [GSH]/[GSSG], as described (Montero et al., 2013), according to equation 2

1-Cys-Grx1pSH + GSSG ⇆ 1-Cys-Grx1pSSG + GSH (equation 2)

and to a K_{ox} of 74 ± 6 (Iversen et al., 2010)

$$R_{GS} = \frac{[GSH]}{[GSSG]} = K_{ox}\frac{[1-Cys-Grx1pSH]}{[1-Cys-Grx1pSSG]}$$

6. Calculation of the absolute glutathione concentration

To calculate the absolute glutathione concentration [GSx], we used $[GSH]^2/[GSSG]$ derived from the E_{GSH} values, and the values of R_{GS} as described (Montero et al., 2013):

$[GSx] = \{([GSH]^2/[GSSG])/R_{GS}) + 2\} \times \{([GSH]^2/[GSSG])/R_{GS}^2)$

7. Quantitative RT-PCR

mRNA was extracted using NucleoSpin RNA (Macherey Nagel). Quantitative RT-PCR used unique oligonucleotide primer pairs designed by the QuantPrime software and assayed for efficiency > 90% and specificity. Total RNA (6 µg) was M-MLV-reversed transcribed using random hexanucleotides as primers, and quantitative PCR was performed in triplicate as described (Desaint et al., 2004).

Supplementary tables

Table S1. List of strains used in this work

Name	**description**	**source**
BY4742	*MATα his3Δ1, leu2Δ0, lys2Δ0, ura3Δ0*	(Brachmann et al., 1998)
BY4742 Δ*ire1*	BY4742 *ire1::kanMX4*	(Brachmann et al., 1998)
BY4742 Δ*hac1*	BY4742 *hac1::kanMX4*	(Brachmann et al., 1998)
BY4742 Δ*gsh1*	BY4742 *gsh1::kanMX4*	(Brachmann et al., 1998)
CKY263	*MATa GAL2 ura3-52 leu2-3,112*	(Frand and Kaiser, 1998)
CKY598	*MATa GAL2 ero1-1 ura3-52 leu2-3,112*	(Frand and Kaiser, 1998)
RSY524	*MATα sec61-2 pep4-3 ade2-1 ura3-52 leu2-3,-112*	(Deshaies and Schekman, 1987)
RSY151	*MATα ura3-52 leu2-3,112 pep4-3 sec63-1*	(Rothblatt et al., 1989)
RSY529	*MATα his4 leu2-3,112 ura3-52 sec62-1*	(Deshaies and Schekman, 1990)
RSY1293	*MATa ura3-1 leu2-3,112 his3-11,15 trp1-1 ade2-1 can1-100 sec61::HIS3* [pDQ1])	(Junne et al., 2006)
EMY101	*MATα trp1-1 ade2 leu2-3,112 ura3 his3-11 can1 sec61::HIS3* [pEM299]	(Trueman et al., 2012)
EMY102	*MATα trp1-1 ade2 leu2-3,112 ura3 his3-11 ssh1::kanMX4 sec61::HIS3* [pEM299]	(Trueman et al., 2012)
YAD337	Δ*egr6* Δ*pdr1* Δ*pdr3*	(Cary et al., 2014)
CKY263/CSY5	*MATa GAL2 ura3-52 leu2-3,112*	(Wang et al., 2014)
CSY275	*MATa GAL2 ura3-52 leu2-3,112 kar2-C63A*	(Wang et al., 2014)

.

Table S2. List of plasmids used in this work

Name	**description**	**source**
pRS315 ER-rxYFP	*CEN LEU2* ER-rxYFP	This study
pRS315 Cyt-rxYFP	*CEN LEU2* Cyt-rxYFP	This study
pRS416 pTEF*HGT1*	*CEN URA3* p*TEF-HGT1*	(Kumar et al., 2011)
pRS304 ER-rxYFP-Grx1	Integrative *LEU2* ERrxYFP-grx1 derived from pJW2011	This study
pTEF415 ER-1-Cys-Grx1	*CEN LEU2* p*TEF*-ER grx1-1cys	This study
pTEF415 Cyt-1-Cys-Grx1	*CEN LEU2* p*TEF*-cyt grx1-1cys	This study
pAF112	*CEN URA3* p*GAL1-ERO1-MYC*	(Sevier et al., 2007)
pCS452	*CEN URA3 pGAL1-ERO1*-MYC*	(Sevier et al., 2007)
pAF85	*CEN LEU2 MYC-ERO1*	(Sevier et al., 2007)
pSM110	pGAL-*SRP54*^{DN} (*TRP1, CEN6/ARSH4*)	(Mutka and Walter, 2001)
pSM131	pGAL-*SRP54* (*TRP1, CEN6/ARSH4*)	(Mutka and Walter, 2001)
pSec61	(2µ, *LEU2*) *SEC61*	This study
pDQ1	(*LEU2 CEN*) *SEC61*	(Junne et al., 2006)
pYC-plac111	(*LEU2 CEN*) *sec61*Δplug	(Junne et al., 2006)
pEM299	pRS316 *URA3 SEC61-V5 (URA3, CEN)*	(Trueman et al., 2012)
pEM635	pRS315 *sec61 N302D*	(Trueman et al., 2012)
pEM634	pRS315 *sec61 N302L*	(Trueman et al., 2012)
pRS315 Sec61	pRS315 *SEC61*	(Tretter et al., 2013)
pRS315 *sec61ΔL7*	pRS315 *sec61*Δ*L7*	(Tretter et al., 2013)
pCS681	pRS315 *KAR2 CEN LEU2*	(Wang et al., 2014)
pCS750	pRS315 *KAR2-C63W CEN LEU2*	(Wang et al., 2014)

Supplemental figures and legends

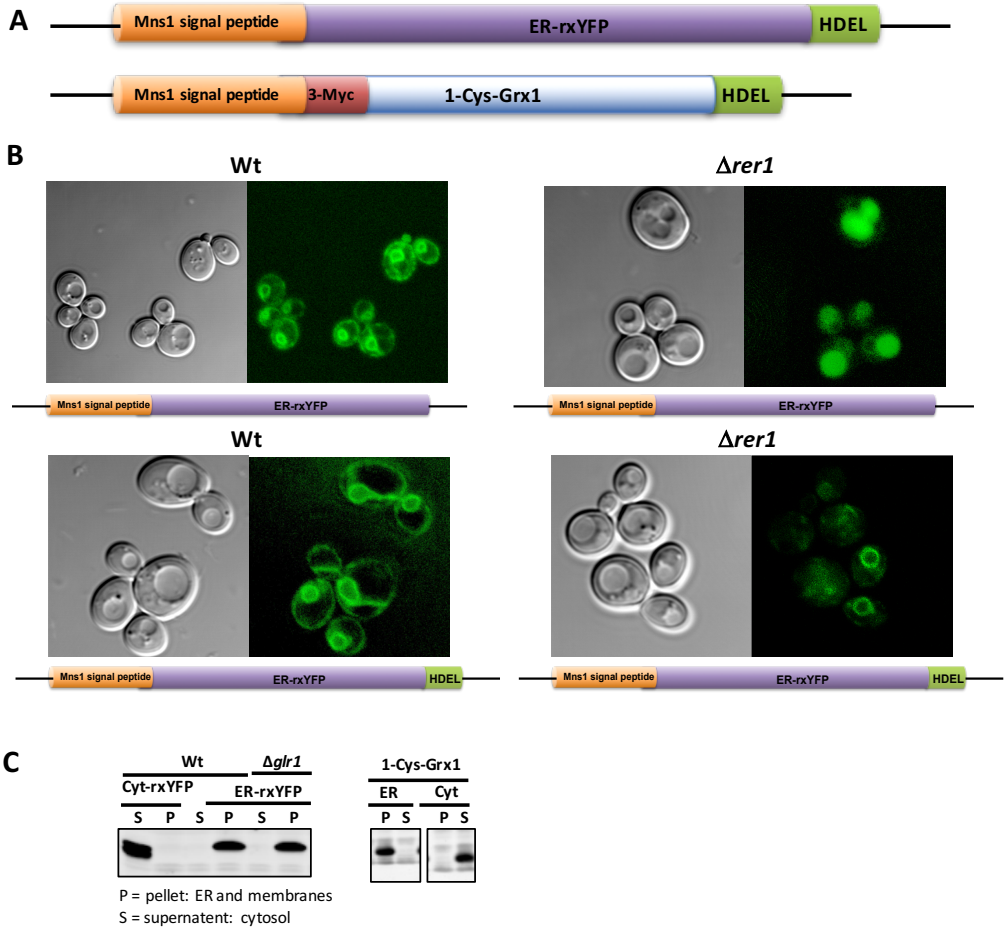

Figure S1. (A) Schematics of ER-rxYFP and ER-1-Cys-Grx1. The cytosolic versions of these probes lack the Mns1 signal sequence and HDEL ER retention signal. These probes are expressed from centromeric plasmid and carry **(i)** the signal sequence of Mns1 and **(ii)** A C-terminal HDEL ER retrieval motif. Mns1 is a type II ER membrane protein with a short 2-3 amino acids cytoplasmic tail, and lacks HDEL or di-lysine ER retention motifs. Instead, by virtue of its N-terminal 23-amino acids signal sequence, which encompasses its transmembrane domain, Mns1 is retrieved form the Golgi back to the ER by the Rer1-dependent pathway (Massaad et al., 1999; Massaad and Herscovics, 2001). **(B)** Each of the two ER localization signals independently localize the probe to the ER: **(Upper left)** ER-rxYFP only carrying the Msn1 signal sequence localizes rxYFP to the ER in Wt cells. **(Upper right)** In Δ*rer1*, ER-rxYFP only carrying the Msn1 signal sequence is mislocalized to the vacuole. **(Lower right)** Further addition of the ER HDEL retrieval motif recovers ER probe localization in Δ*rer1* by a different pathway. **(Lower left)** The probe carrying both the Msn1 signal sequence and HDEL motif displays an ER localization in Wt cells. Exponential phase grown cells were imaged using a Leica TCS SP2 confocal scanning microscope with an excitation wavelength for GFP at 488 nm and selection of emitted light of 500–570 nm. **(C)** Cellular fractionation between cytosol (S) and membranes (P) indicate the correct localization of ER-rxYFP and ER-1-Cys-Grx1 in the ER, and of Cyt-rxYFP and Cyt-1-Cys-Grx1 in the cytosol of Wt cells or Δ*glr1*, as indicated. Spheroplasts obtained by treatment of a cell suspension with

Zymolyase were disrupted by osmotic shock. After discarding non-disrupted cells by low speed centrifugation (2000 g), the supernatent was fractionated by centrifugation at 13,000 *g* between pellet, containing membranes (P), and supernatant, containing the cytosol (S). Proteins were separated by SDS-PAGE and immunoblotted, using anti-GFP (rxYFP) or anti-Myc (1-Cys-Grx1) antibodies.

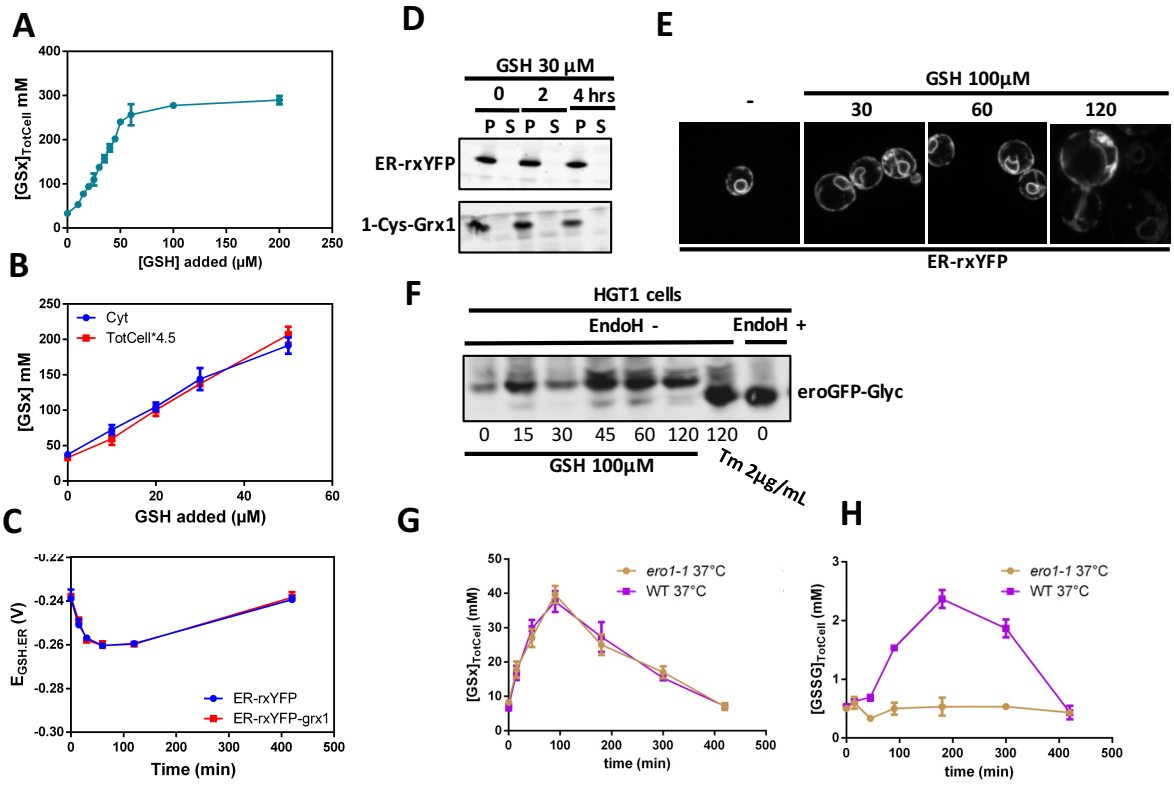

Figure S2. (A) Total GSx (GSH + 2GSSG) measured by the DNTB assay in HGT1 cells incubated 1 h with the indicated amount of GSH. **(B)** $[GSx]_{TotCell}$ is used as proxy of $[GSx]_{Cyt}$. $[GSx]_{Cyt}$ and $[GSx]_{TotCell}$ measured in HGT1-Δ*glr1* cells incubated 1 h with the indicated amount of GSH, align together after multiplying $[GSx]_{TotCell}$ by 4.5. **(C)** Comparison of E_{GSH} measured with either ER-rxYFP or ER-rxYFP-Grx1 in HGT1 cells incubated with 30 µM GSH for the indicated time. **(D)** ER-rxYFP and ER-1-Cys-Grx1 localize to the ER in HGT1 cells incubated 2 and 4 h with 30 µM GSH, as shown by subcellular fractionation (see Fig. S1C). **(E)** By fluorescence microscopy, ER-rxYFP localize to the ER in HGT1 cells incubated 2 h with the indicated amount of GSH. **(F)** ER localization of eroGFP-Glyc is shown by its glycosylation state. In eroGFP (Merksamer et al., 2008), there is a 15-amino acid glycosylation site before the HDEL. Lysates from HGT1 cells carrying eroGFP-Glyc and incubated with 100 µM GSH for the indicated time, or treated with 2 µg/mL of tunicamycin (Tm) for 2 hrs, were resuspended in lysis buffer (50mM Tris-HCl pH 8 and 2% SDS), boiled 5 minutes and centrifuged at 10,000 g. Supernatants were treated with or without EndoH, as described (Kumar et al., 2011), and proteins were separated by SDS-PAGE and immunoblotted with anti-GFP antibodies. In GSH-treated samples eroGFP-Glyc is fully glycosylated throughout the time-course, indicating ER probe localization. As controls, lysates treated with EndoH, or from cells treated with tunicamycin, which inhibits glycosylation, were used. **(G, H)** HGT1-dependent GSH accumulation leads to GSSG production that originates from Ero1. Total cellular [GSx] (G) and [GSSG] (H) measured by the DTNB assay in HGT1 and HGT1-*ero1-1* cells incubated at 37 °C for 1 h prior to and during the indicated time after addition of 30 µM GSH. In A-C, G, H, each value is the mean of three independent biological replicas ± standard deviation (s.d.).

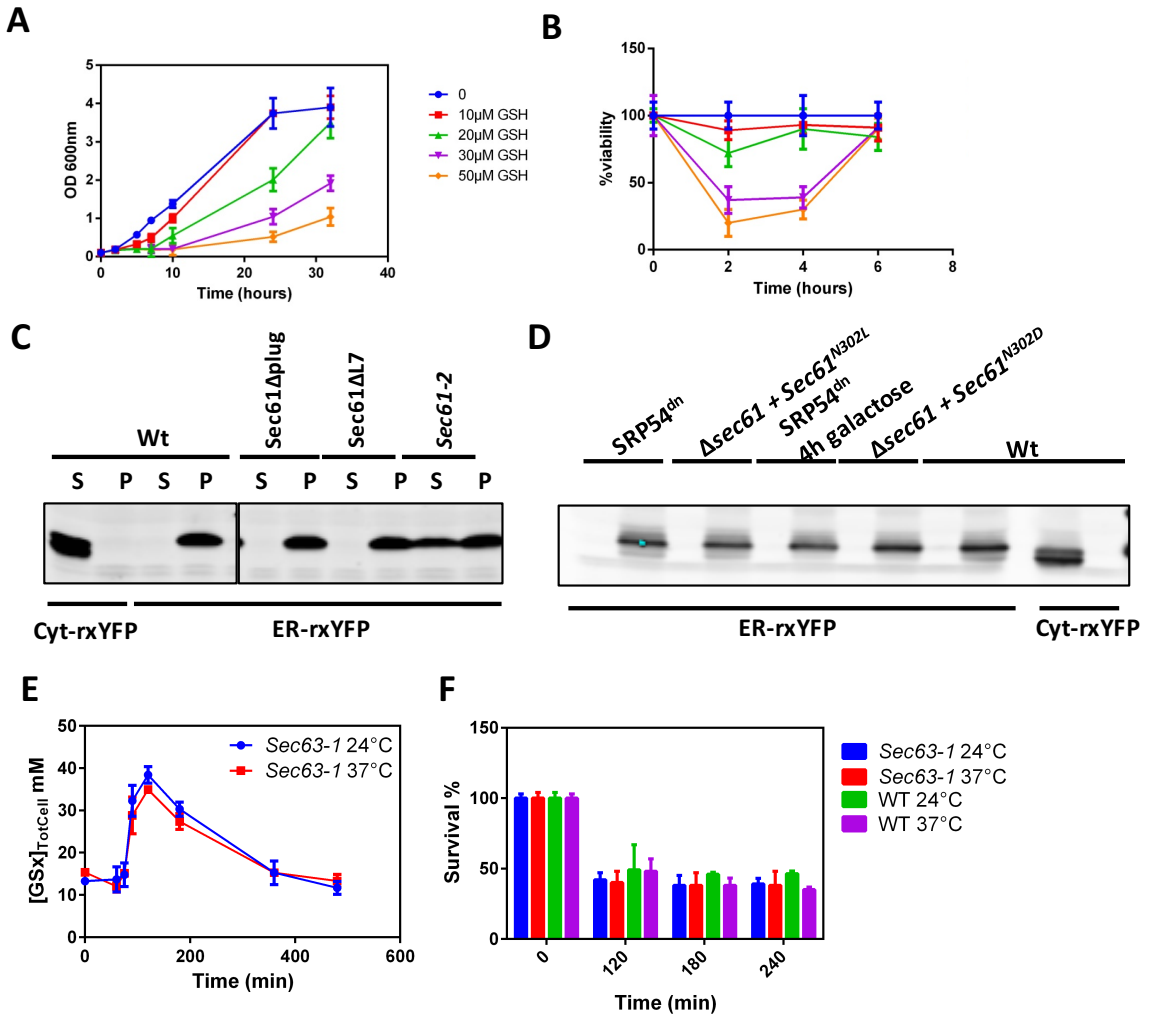

Figure S3. (A, B) HGT1-dependent GSH cellular accumulation causes growth inhibition and cell death in a manner proportional to the amount of added GSH. **(A)** HGT1 cells were incubated with the indicated amount of GSH and growth was recorded at the indicated time by the OD_{600}. **(B)** HGT1 cells were incubated with the indicated amount of GSH and survival was determined at the indicated time. **(C, D)** Localization of ER-rxYFP or Cyt-rxYFP in HGT1 cells or in cells with the indicated genetic background carrying HGT1, as assayed by subcellular fractionation (see Fig. S1C, for the method). For HGT1 cells expressing Gal1-$SRP54^{dn}$, localization was assayed 4 h after switching from glucose to galactose. **(E, F)** HGT1-dependent cellular GSH accumulation and toxicity in *sec63-1* is similar at the non-restrictive and restrictive temperatures. (E) Accumulation of GSH by HGT1-*sec63-1* ($[GSx]_{TotCell}$) measured by the DTNB enzyme assay as a function of time upon incubation with 30 μM GSH at 24 and 37°C. (F) GSH survival assay. HGT1-expressing *sec63-1* cells grown to exponential phase at 24 °C, and switched to 37 °C or left at 24 °C as indicated 45 min prior to adding GSH (30 μM) to the medium. In A, B, E, F, each value displayed is the mean of three independent biological replicas ± standard deviation (s.d.).

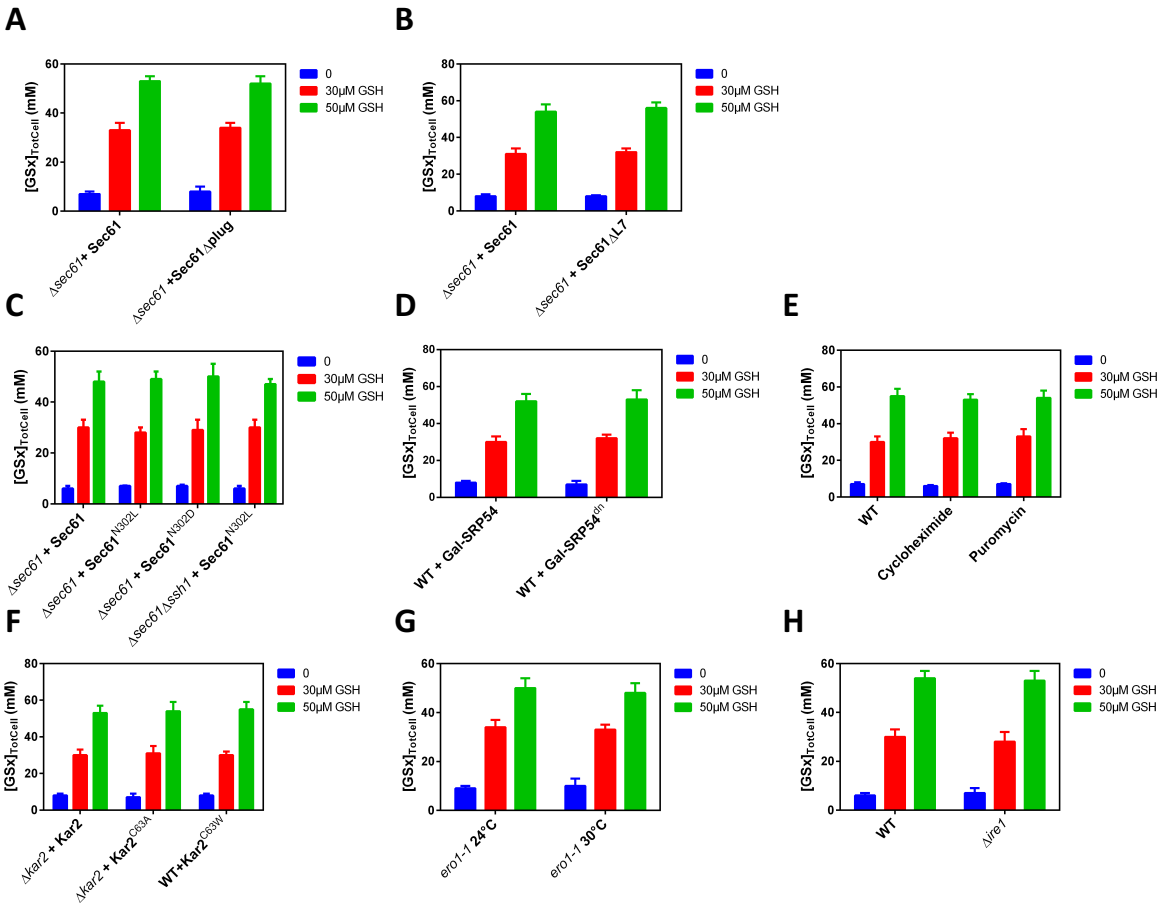

Figure S4. HGT1-dependent GSH cellular accumulation was measured by the DTNB enzyme assay after a 1-h incubation of the indicated cells in the presence of 30 and 50 µM GSH. **(A)** HGT1-Δ*sec61* expressing *SEC61* or *SEC61*-Δplug. **(B)** HGT1-Δ*sec61* expressing *SEC61* or *SEC61ΔL7*. **(C)** HGT1-Δ*sec61* or HGT1-Δ*sec61*Δ*ssh1* expressing *SEC61*, or *sec61N302L*, or *sec61N302D*, as indicated. **(D)** HGT1 cells expressing *Gal1-SRP54*, or *Gal1-SRP54*^{dn}, as indicated, after 3 h in galactose medium. **(E)** HGT1 cells treated with cycloheximide (CHX) (200 µg/mL) for 10 min or with puromycine (2 mM) for 15 min. **(F)** HGT1-Δ*kar2* expressing Wt *KAR2*, or *kar2*^{C63A} or Wt HGT1 cells expressing *KAR2*^{C63W}, as indicated. **(G)** HGT1-*ero1-1* grown at 24°C or 37°C, 1 h prior to GSH addition. **(H)** HGT1 or HGT1-Δ*ire1* cells, as indicated. Each value displayed is the mean of three independent biological replicas ± standard deviation (s.d.).

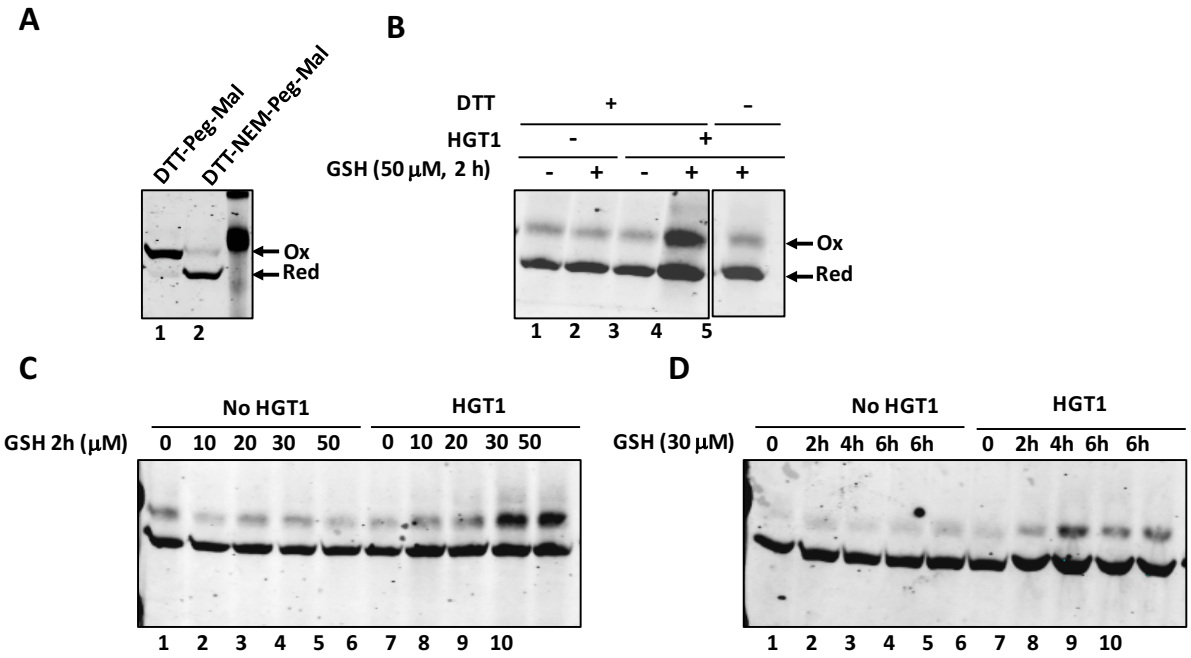

Figure S5. **Control experiments for the method of differential labeling of Cys residue used to monitor Kar2 oxidation, and showing that in the absence of HGT1, GSH does not triggers Kar2 oxidation. (A)** TCA extracts of untreated cells were reduced by DTT, alkylated or not by NEM, as indicated, and then alkylated by PEG-Mal: prior alkylation by NEM prevents alkylation by PEG-Mal (compare the two lanes). The migration of NEM-alkylated Kar2 (lane 1, mimics reduced protein), and PEG-Mal-Kar2 (lane 2, mimics oxidized protein) is shown. **(B)** Cells carrying or not HGT1, as indicated, were exposed or not to GSH (50 µM) for 2 h, as indicated. TCA extracts were alkylated with NEM, reduced or not by DTT, as indicated, and alkylated by PEG-Mal: absence of the DTT reduction step prevents Cys residue alkylation by PEG-Mal (compare lanes 4 and 5), which indicates that PEG-Mal modifies residues that are in a form sensitive to DTT reduction *in vivo*, such as a sulfenic acid or glutathionylated form. In cells that do not overexpress HGT1, GSH does not trigger Kar2 oxidation (compare lanes 2 and 4), as also shown below. **(C, D)** Kar2 does not become oxidized in response to GSH in cells that do not express HGT1. Exponentially growing cells that expressed or not HGT1, as indicated, were exposed during 2 h to increasing amounts of GSH, as indicated (C), or to 30 µM GSH during the time indicated (D). TCA extracts were alkylated with NEM, then reduced and alkylated with PEG-maleimide.

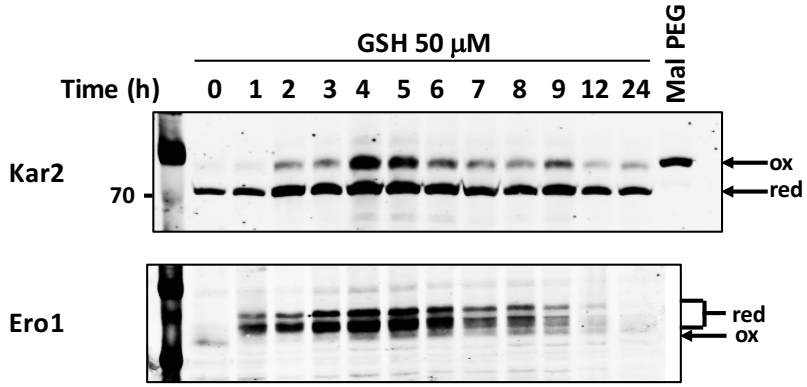

Figure S6. The ER import of GSH triggers the reductive activation of Ero1, and the oxidation of Kar2. Lysates of HGT1 cells expressing Myc-tagged Ero1 exposed to 50 μM GSH for the indicated times were processed for differential labeling of reduced *vs* oxidized residues by NEM/PEG-Mal (upper gel), or alkylated by NEM (lower gel), separated by reducing (upper gel) or non-reducing (lower gel) SDS-PAGE, respectively, followed by western blot with anti-Kar2 (upper gel) or anti-Myc (lower gel) antibodies. The last lane of the upper gel shows the oxidized Kar2 control, obtained by PEG-Mal alkylation after DTT reduction, without prior NEM alkylation. Exposure of HGT1 cells to GSH triggers Ero1 reduction and Kar2 oxidation, with the former preceding the latter. After several hrs, Ero1 and Kar2 return to their oxidized or reduced states, respectively, with Kar2 reduction occurring later than Ero1 oxidation. UPR induction parallels the protein redox changes, as shown by the changes in Ero1 and Kar2 protein levels.

Supplemental references

Bjornberg, O., Ostergaard, H., and Winther, J.R. (2006). Measuring intracellular redox conditions using GFP-based sensors. Antioxid Redox Signal *8*, 354-361.

Brachmann, C.B., Davies, A., Cost, G.J., Caputo, E., Li, J., Hieter, P., and Boeke, J.D. (1998). Designer deletion strains derived from Saccharomyces cerevisiae S288C: a useful set of strains and plasmids for PCR-mediated gene disruption and other applications. Yeast *14*, 115-132.

Cary, G.A., Yoon, S.H., Torres, C.G., Wang, K., Hays, M., Ludlow, C., Goodlett, D.R., and Dudley, A.M. (2014). Identification and characterization of a drug-sensitive strain enables puromycin-based translational assays in Saccharomyces cerevisiae. Yeast *31*, 167-178.

Delaunay, A., Isnard, A.D., and Toledano, M.B. (2000). H2O2 sensing through oxidation of the Yap1 transcription factor. EMBO J *19*, 5157-5166.

Desaint, S., Luriau, S., Aude, J.C., Rousselet, G., and Toledano, M.B. (2004). Mammalian antioxidant defenses are not inducible by H2O2. J Biol Chem *279*, 31157-31163.

Deshaies, R.J., and Schekman, R. (1987). A yeast mutant defective at an early stage in import of secretory protein precursors into the endoplasmic reticulum. J Cell Biol *105*, 633-645.

Deshaies, R.J., and Schekman, R. (1990). Structural and functional dissection of Sec62p, a membrane-bound component of the yeast endoplasmic reticulum protein import machinery. Mol Cell Biol *10*, 6024-6035.

Frand, A.R., and Kaiser, C.A. (1998). The ERO1 gene of yeast is required for oxidation of protein dithiols in the endoplasmic reticulum. Mol Cell *1*, 161-170.

Hu, J., Dong, L., and Outten, C.E. (2008). The redox environment in the mitochondrial intermembrane space is maintained separately from the cytosol and matrix. J Biol Chem *283*, 29126-29134.

Iversen, R., Andersen, P.A., Jensen, K.S., Winther, J.R., and Sigurskjold, B.W. (2010). Thiol-disulfide exchange between glutaredoxin and glutathione. Biochemistry *49*, 810-820.

Junne, T., Schwede, T., Goder, V., and Spiess, M. (2006). The plug domain of yeast Sec61p is important for efficient protein translocation, but is not essential for cell viability. Mol Biol Cell *17*, 4063-4068.

Kumar, C., Igbaria, A., D'Autreaux, B., Planson, A.G., Junot, C., Godat, E., Bachhawat, A.K., Delaunay-Moisan, A., and Toledano, M.B. (2011). Glutathione revisited: a vital function in iron metabolism and ancillary role in thiol-redox control. EMBO J *30*, 2044-2056.

Massaad, M.J., Franzusoff, A., and Herscovics, A. (1999). The processing alpha1,2-mannosidase of Saccharomyces cerevisiae depends on Rer1p for its localization in the endoplasmic reticulum. Eur J Cell Biol *78*, 435-440.

Massaad, M.J., and Herscovics, A. (2001). Interaction of the endoplasmic reticulum alpha 1,2-mannosidase Mns1p with Rer1p using the split-ubiquitin system. J Cell Sci *114*, 4629-4635.

Merksamer, P.I., Trusina, A., and Papa, F.R. (2008). Real-time redox measurements during endoplasmic reticulum stress reveal interlinked protein folding functions. Cell *135*, 933-947.

Montero, D., Tachibana, C., Rahr Winther, J., and Appenzeller-Herzog, C. (2013). Intracellular glutathione pools are heterogeneously concentrated. Redox Biol *1*, 508-513.

Mutka, S.C., and Walter, P. (2001). Multifaceted physiological response allows yeast to adapt to the loss of the signal recognition particle-dependent protein-targeting pathway. Mol Biol Cell *12*, 577-588.

Ostergaard, H., Tachibana, C., and Winther, J.R. (2004). Monitoring disulfide bond formation in the eukaryotic cytosol. J Cell Biol *166*, 337-345.

Rothblatt, J.A., Deshaies, R.J., Sanders, S.L., Daum, G., and Schekman, R. (1989). Multiple genes are required for proper insertion of secretory proteins into the endoplasmic reticulum in yeast. J Cell Biol *109*, 2641-2652.

Sevier, C.S., Qu, H., Heldman, N., Gross, E., Fass, D., and Kaiser, C.A. (2007). Modulation of cellular disulfide-bond formation and the ER redox environment by feedback regulation of Ero1. Cell *129*, 333-344.

Tretter, T., Pereira, F.P., Ulucan, O., Helms, V., Allan, S., Kalies, K.U., and Romisch, K. (2013). ERAD and protein import defects in a sec61 mutant lacking ER-lumenal loop 7. BMC Cell Biol *14*, 56.

Trueman, S.F., Mandon, E.C., and Gilmore, R. (2012). A gating motif in the translocation channel sets the hydrophobicity threshold for signal sequence function. J Cell Biol *199*, 907-918.

Wang, J., Pareja, K.A., Kaiser, C.A., and Sevier, C.S. (2014). Redox signaling via the molecular chaperone BiP protects cells against endoplasmic reticulum-derived oxidative stress. Elife *3*, e03496.